2026, Scienceline Publication
World's Veterinary Journal
World Vet J, 16(1): 127-138.
ISSN 2322-4568

DOI: https://dx.doi.org/10.54203/scil.2026.wvj12
PII: S232245682600012-16

Effects of Matrix Metalloproteinase-9-Dependent Extracellular Matrix on Remodeling Underlie Accelerated Skin Aging in Streptozotocin-induced Diabetic Rats

Ruri Eka Maryam Mulyaningsih[1,5], Neng Tine Kartinah[2], Ani Retno Prijanti[3], Christian Marco Hadi Nugroho[4], and Desak Gede Budi Krisnamurti [6]*

[1]*Doctoral Program of Biomedical Sciences, Faculty of Medicine, Universitas Indonesia, Jakarta, Indonesia*
[2]*Department of Medical Physiology, Faculty of Medicine, Universitas Indonesia, Jakarta, Indonesia*
[3]*Department of Biochemistry and Molecular Biology, Faculty of Medicine, Universitas Indonesia, Jakarta, Indonesia*
[4]*Research and Development Unit, PT Medika Satwa Laboratories, Bogor, Indonesia*
[5]*Faculty of Medicine, Universitas Swadaya Gunung Jati, Cirebon, Indonesia*
[6]*Department of Medical Pharmacy, Faculty of Medicine, Universitas Indonesia, Jakarta, Indonesia*

*Corresponding author's Email: desak.gede@ui.ac.id

ORIGINAL ARTICLE
Received: December 28, 2025
Revised: January 30, 2026
Accepted: February 24, 2026
Published: March 25, 2026

ABSTRACT

Type 2 diabetes mellitus (T2DM) is a chronic metabolic disorder associated with progressive aging-related alterations in multiple organs, including the skin. Nonetheless, the specific structural and molecular changes that cause skin aging in diabetes remain poorly understood in preclinical animal models. The present study aimed to establish a rat model of T2DM-induced skin aging and to investigate the relationship between matrix metalloproteinase-9 (MMP-9) expression and dermal extracellular matrix (ECM) remodeling in diabetic skin aging. A total of 12 male Sprague-Dawley rats, aged 8-9 weeks and weighing 180-250 g, were assigned to the control and T2DM groups. Rats in the T2DM group received an 8-week high-fat diet (45% fat calories) with 40% fructose, followed by low-dose streptozotocin (25 mg/kg, IP) injection to induce diabetes. Metabolic phenotype was validated using fasting blood glucose and a 2-hour post-glucose measurement. After 16 weeks, dorsal skin was collected for histological evaluation, including measurements of epidermal/dermal thickness, collagen area, and fibroblast counts, as well as molecular analysis. The MMP-9 was measured using a sandwich enzyme-linked immunosorbent assay. Diabetic rats developed sustained hyperglycemia and increased body weight, confirming a T2DM-like metabolic phenotype. Histological analysis demonstrated a significant increase in dermal thickness and a marked reduction in dermal collagen density in diabetic skin, whereas epidermal thickness and fibroblast counts were not significantly altered. The MMP-9 concentration in diabetic dermal homogenates was elevated compared with that in the control group. The current findings demonstrated that T2DM in rats was associated with early dermal extracellular matrix remodeling, characterized by increased MMP-9 levels, decreased collagen density, and dermal thickening, suggesting an association between chronic hyperglycemia and altered dermal matrix homeostasis.

Keywords: Collagen, Dermal extracellular matrix, Matrix metalloproteinase-9, Rat, Skin aging, Type 2 diabetes mellitus

INTRODUCTION

Type 2 diabetes mellitus (T2DM) is characterized by chronic hyperglycemia that drives systemic biological disturbances affecting multiple organs, including the skin (Brownlee, 2001). In clinical practice, individuals with T2DM frequently exhibit cutaneous manifestations such as accelerated aging-like features, increased dermal rigidity, and impaired wound healing (Moraes et al., 2023). Such skin alterations are associated with disturbances in extracellular matrix (ECM) homeostasis and functional impairment of dermal fibroblasts (Argyropoulos et al., 2016; Zhu et al., 2022). Epidemiological and clinical studies have indicated that individuals with long-term or poorly managed diabetes often develop skin characteristics that resemble accelerated aging, which can negatively impact tissue resilience and overall quality of life (Berlanga-Acosta et al., 2020; Shin et al., 2019).

From a histological perspective, the dermis is a primary target of diabetic skin changes. The structural integrity of the dermis depends primarily on the ECM, which is composed of collagen fibers produced and maintained by dermal fibroblasts. Under diabetic conditions, disturbances in ECM homeostasis have been associated with altered collagen organization, impaired matrix turnover, and functional changes in fibroblasts, which may collectively contribute to increased tissue stiffness and reduced repair capacity (Argyropoulos et al., 2016; Zhu et al., 2022). Such alterations in

To cite this paper: Mulyaningsih REM, Kartinah NT, Prijanti AR, Nugroho CMH, and Krisnamurti DGB (2026). Effects of Matrix Metalloproteinase-9-Dependent Extracellular Matrix on Remodeling Underlie Accelerated Skin Aging in Streptozotocin-induced Diabetic Rats. *World Vet. J.,* 16(1): 127-138. DOI: https://dx.doi.org/10.54203/scil.2026.wvj12

extracellular matrix organization and fibroblast function suggest that dermal remodelling may play an important role in the aging-like skin features observed in diabetes.

At the molecular level, the histological and structural alterations are closely linked to chronic metabolic dysregulation. Chronic hyperglycemia promotes the formation and accumulation of advanced glycation end-products (AGEs), which modify ECM proteins through non-enzymatic cross-linking. Interaction of AGEs with the receptor for advanced glycation end-products (RAGEs) activates inflammatory signaling pathways, including NFκB and MAPK, leading to increased oxidative stress and dysregulated expression of matrix metalloproteinases (MMPs) (Chen et al., 2023). Among these enzymes, matrix metalloproteinase-9 (MMP-9) has received particular attention due to its collagenolytic activity and its association with abnormal dermal remodeling and impaired wound healing in diabetic conditions (Zhou et al., 2021; Zhu et al., 2022). Meanwhile, dermal fibroblasts exposed to chronic metabolic stress develop a dysfunctional or senescence-like phenotype. This phenotype includes decreased collagen production and a proinflammatory, matrix-degrading secretory profile known as the senescence-associated secretory phenotype (SASP) (Ogata et al., 2021; Wlaschek et al., 2021).

Despite the extensive use of T2DM rat models to study metabolic aspects of diabetes mellitus, the comprehensive characterization of diabetes-related skin aging in rats remains limited, as many experimental studies have mainly focused on glycemic control or systemic metabolic outcomes, while skin structural and molecular changes are often less explored (Sanapalli et al., 2021). Therefore, establishing a stable and reproducible animal model that accurately reflects diabetic skin pathology is essential for advancing mechanistic and therapeutic study in this field (Pandey et al., 2023). Thus, the present study aimed to establish and characterize the structural and molecular features of diabetes-associated skin aging in Sprague-Dawley rat models induced by a high-fat, high-fructose diet followed by low-dose streptozotocin (STZ) administration, with particular focus on dermal ECM remodeling and MMP-9 expression under chronic hyperglycemia conditions.

MATERIALS AND METHODS

Ethical approval

All animal procedures were approved by the Ethics Committee, Faculty of Medicine, Indonesia University, Indonesia (Approval No. KET-562/UN2.F1/ETIK/PPM. 00.02/2022). All experiments were performed in accordance with institutional regulations and national guidelines for the care and use of laboratory animals, and complied with internationally accepted principles for animal research (Percie du Sert et al., 2020).

Animals and experimental design

The present study was designed as an *in vivo* experiment using Sprague-Dawley rats to investigate diabetes-associated skin aging. Male Sprague-Dawley rats were obtained at 8-9 weeks of age, with an initial body weight of 180-250 g. Prior to the experiment, all rats were acclimatized for 10 days and maintained under controlled conditions of 50-60% humidity, 22 ± 2°C, and a 12-hour light/dark cycle with unrestricted access to food and water. Baseline fasting blood glucose (FBG) and 2-hour post-glucose levels were measured before the intervention to confirm normoglycemic status, and only rats with normal glycemic values were included in the study.

A total of 12 male rats were randomly assigned to two experimental groups, including a control group of four rats and a T2DM group of eight rats. Rats in the control group were maintained on a standard laboratory diet throughout the study period. Rats in the T2DM group (diabetic) received a laboratory-prepared high-fat diet designed to provide approximately 45% of total caloric intake from fat (Kartinah et al., 2022). The diet consisted of 100 g mixture, including 60 g of standard rodent chow (Rat Bio®, PT Citra Ina Feedmill, Jakarta, Indonesia), 15 g of beef tallow, 13 g of egg yolk powder (Y1105, Egg Products Export Limited, Tamil Nadu, India), 10 g of skim milk casein powder (NZMP®, Fonterra Co-operative Group, Auckland, New Zealand), and 2 g of powdered sugar. All ingredients were thoroughly homogenized prior to feeding. In addition, rats were provided with a freshly prepared 40% fructose solution for eight weeks to induce insulin resistance. At the end of the eight-week dietary induction period, T2DM rats were administered a low dose intraperitoneal injection of streptozotocin (25 mg/kg body weight), freshly dissolved in 100 mM citrate buffer (pH 4.5), to induce chronic hyperglycemia. Seventy-two hours after streptozotocin administration, FBG and 2-hour post-glucose measurements were performed. Animals were classified as diabetic only when both parameters met the predefined glycemia criteria. The induction protocol was adapted from a standard and widely used diet and streptozotocin-induced T2DM model (Barrière et al., 2018).

After confirming the diabetic status in T2DM-induced rats, they remained under their respective experimental conditions for another eight weeks, extending the overall study duration to 16 weeks.

Metabolic measurements

Body weight measurements were recorded every four weeks from the end of acclimatization until the completion of the 16-week experimental period. The FBG and 2-hour post-glucose measurements were performed prior to the dietary intervention, at week eight (after completion of high-fat/high-fructose feeding), and at week 16 (study endpoint following diabetes confirmation). For glucose assessment, rats were fasted overnight (12 hours) and given an oral glucose load of 2 g/kg body weight using a sterile feeding needle. Blood glucose levels were measured at fasting (0 minutes) and 120 minutes after glucose administration. No intermediate time points were collected. Blood glucose concentrations were determined using a validated handheld glucometer (EasyTouch®, Bioptic Technology, Taiwan), which has been widely used in experimental diabetes study (Nindita et al., 2023).

Diabetes status in experimental animals was categorized using modified clinical glycemic thresholds to ensure relevance to human conditions. Rats were classified as diabetic when FBG levels exceeded 126 mg/dL (7.0 mmol/L) and 2-hour post-glucose levels exceeded 200 mg/dL (11.1 mmol/L), consistent with the criteria proposed by the American Diabetes Association and commonly applied in rodent diabetes models (Liu et al., 2020; Percie du Sert et al., 2020). The selected glycemic thresholds were aligned with the metabolic characteristics of the diet-low-dose streptozotocin model, which reflected moderate, sustained hyperglycemia typical of type 2 diabetes rather than the severe insulin-deficient phenotype observed in high-dose streptozotocin models.

Tissue collection

At week 16, animals were anesthetized with an intraperitoneal injection of ketamine (80 mg/kg body weight) combined with xylazine (10 mg/kg body weight). The mentioned doses were selected based on established protocols to achieve deep surgical anesthesia (Van Pelt, 1977). Following confirmation of adequate anesthesia, animals were humanely euthanized in compliance with institutional ethical guidelines and the recommendation of the American Veterinary Medical Association (AVMA, 2020). Dorsal skin samples were collected from the standardized mid-dorsal region after clipping and shaving of dorsal hair. To minimize sampling variability, a uniform tissue area of approximately 2 cm × 2 cm was excised from each animal using consistent anatomical positioning. Underlying skeletal muscle was carefully excluded during dissection, and excess subcutaneous adipose tissue was gently trimmed to minimize fat inclusion while preserving the full-thickness dermis (Wells et al., 2010).

Anatomical orientation was preserved during fixation and paraffin embedding by positioning the epidermal surface upward. Sections were cut perpendicular to the epidermal surface to ensure consistent and reproducible measurements of epidermal and dermal thickness. Thickness measurements were obtained from multiple non-overlapping fields within each section, and the mean value per animal was used for statistical analysis.

For histological analysis, tissue samples were immediately immersed in 10% neutral-buffered formalin and fixed for 24 hours at room temperature. Following fixation, samples were rinsed in phosphate-buffered saline (PBS, pH = 7.4), dehydrated through a graded ethanol series, and embedded in paraffin. Serial sections of 5 µm thickness were prepared and stained with hematoxylin and eosin (H&E) for general morphology and Masson's Trichrome to visualize collagen fibers (Arnal-Forné et al., 2024). All samples were processed immediately after the fixation period to minimize fixation-related variability.

For biochemical analysis, specifically protein extraction, a nearby section of the standardized dorsal skin area (trimmed of hair and underlying muscle tissue) was rapidly frozen and stored at -80°C until subsequent homogenization and enzyme-linked immunosorbent assay (ELISA).

Histological analysis

Histological analyses were conducted using ImageJ software by independent observers blinded to group assignment. For each animal, five non-overlapping high-power fields (HPF) were randomly chosen from distinct dermal areas within each section to ensure representative sampling. The average of these five HPF per animal was calculated and used for statistical analysis.

Epidermal thickness was measured using H&E-stained sections as the perpendicular distance from the stratum basale to the outermost layer of stratum corneum, using established histomorphology methods (Giangreco et al., 2010). Dermal thickness was assessed using H&E-stained sections by measuring the perpendicular distance from the derma-epidermal junction to the histologically recognizable dermal-hypodermal interface. This boundary was determined by the transition from the dense collagenous connective tissue of the dermis to the subcutaneous adipose tissue (Giangreco et al., 2010; Schneider et al., 2012). Fibroblast counts were assessed using H&E-stained sections by manually counting the purple spindle-shaped, nucleated cells scattered among the collagen and elastin fibers within the dermis. Counts were performed in each square in five randomly selected non-overlapping HPF (400x) per section, while excluding the perivascular region and adnexal structures. Mean values were calculated for each sample (Varani et al., 2006).

Masson's Trichrome staining was used to visualize collagen. Masson's Trichome-stained sections were randomly selected and imaged. The dermal region was manually delineated in each image, and dermal collagen density was quantified using ImageJ software (Schneider et al., 2012; Nan et al., 2025).

Homogenization and protein extraction

Skin tissue samples stored at -80°C were thawed on ice prior to protein extraction. Each sample was briefly rinsed in cold PBS (pH = 7.4) to remove surface debris and residual blood. Approximately 100 mg of dorsal skin tissue, free hair, and underlying muscle were homogenized in 900 µL of ice-cold PBS (pH = 7.4) supplemented with 1 mM phenylmethylsulfonyl fluoride (PMSF), a serine protease inhibitor, to minimize nonspecific proteolytic degradation during homogenization (tissue-to-buffer ratio=1:9, w/v). As MMP-9 levels were quantified using an ELISA-based assay to measure total protein concentration rather than enzymatic activity, MMP-specific inhibition during homogenization was not required (Powers et al., 2002).

Skin tissue was homogenized on ice using a rotor-stator tissue homogenizer (Tokyo Rikakikai Co., Ltd., Tokyo, Japan). Samples were processed at 7,000 rpm in repeated short cycles for a total of approximately 7-10 minutes, with intermittent ice cooling between cycles to prevent heat-induced protein degradation, until a uniform suspension was obtained. The homogenates were subsequently centrifuged at 5,000x g (relative centrifugal force) for 5 minutes at 4°C, resulting in separation into a clear aqueous supernatant and a pellet containing insoluble cellular debris. The aqueous supernatant, representing the soluble protein fraction, was carefully collected for subsequent biochemical and immunoassay analyses. Any superficial lipid layer, when present, was carefully avoided during supernatant collection. Supernatant samples were stored at -80°C until further analysis (Zhu et al., 2022).

During tissue collection, hypodermal adipose tissue was carefully trimmed to ensure that only dermal skin tissue was included for biochemical analyses. All procedures were conducted at cold temperatures to preserve protein integrity and minimize post-homogenization proteolysis.

Total protein concentration was determined using the Bradford assay with bovine serum albumin as the standard (Bradford, 1976). Preliminary dilution optimization was performed to ensure that protein concentrations fell within the linear detection range of the Bradford assay and within the dynamic range of the ELISA kit. Samples were diluted with PBS (pH = 7.4) according to the determined dilution factors to achieve comparable total protein input prior to quantification of MMP-9.

Matrix Metalloproteinase-9 quantification

Quantitative analysis of MMP-9 from supernatant skin tissue homogenates was measured using a commercially available sandwich Rat MMP-9 ELISA kit (FineTest®, Wuhan Fine Biotech Co., China; Catalog No. ER0139), according to the manufacturer's instructions. All samples were analyzed at equivalent total protein concentrations, as determined by the Bradford assay, to minimize inter-sample variability. Samples and standards were added to microplate wells pre-coated with anti-MMP-9 antibodies, followed by incubation with a biotin-conjugated detection antibody and horseradish peroxidase-streptavidin. After thorough washing steps, the tetramethylbenzidine substrate was added to initiate color development, which was subsequently stopped with sulfuric acid. Absorbance was measured at 450 nm using a microplate reader (Bio-Rad Laboratories, CA, USA), and MMP-9 concentrations were determined from a standard curve generated using known concentrations of recombinant protein (Zhu et al., 2022). The MMP-9 levels were normalized to total protein content and expressed as pg/mg protein. All samples and standards were assayed in duplicate, and mean absorbance values were used to calculate concentrations.

Statistical analysis

All quantitative data were presented as mean ± standard deviation (SD). Data distribution was assessed for normality using the Shapiro–Wilk test. Comparison between the two groups was performed using a t-test for normally distributed data, or a Mann-Whitney test for non-parametric data. All samples were analyzed in duplicate, and the coefficient of variation (CV) between replicates was used to monitor assay precision. Statistical analyses were performed using SPSS software (version 27.0; IBM Corp., USA). A two-tailed p-value of less than 5% was considered statistically significant ($p < 0.05$).

RESULTS

For all metabolic, histological, and biochemical analyses, all animals were included (control, n = 4; T2DM, n = 8). No animals were excluded from any part of the study analysis.

Metabolic phenotype

All rats in the T2DM group developed sustained hyperglycemia between weeks 8 and 16 and maintained elevated blood glucose levels throughout the experimental period. After diabetes induction at week 8, FBG and 2-hour post-glucose levels increased progressively and remained elevated until week 16 in the T2DM group. At week 16, FBG in diabetic rats (372.3 ± 143.4 mg/dL) was significantly higher than in the control group (184.8 ± 15.1 mg/dL; $p < 0.05$; Figure 1A). Consistently, the 2-hour post-glucose measurement indicated significantly impaired glucose clearance in the T2DM group, indicated by markedly higher plasma glucose levels at 2 hours after the glucose load (404.1 ± 132.9 mg/dL versus 150.0 ± 39.6 mg/dL; $p < 0.05$; Figure 1B). Although fasting glucose levels in the control group were slightly higher than the usual reference ranges observed in non-experimental settings, all animals were maintained under identical environmental and dietary conditions. The T2DM group had significantly higher fasting and post-glucose levels than the control group ($p < 0.05$). In addition to hyperglycemia, body weight increased significantly in the diabetic rats (315.8 ± 43.4 g) by week 16 compared to the control group (181.8 ± 49.5 g; $p < 0.05$; Figure 1C). The present findings confirmed successful induction of a T2DM-like metabolic phenotype, consistent with rat-specific glycemic thresholds adapted from clinical criteria (Barrière et al., 2018).

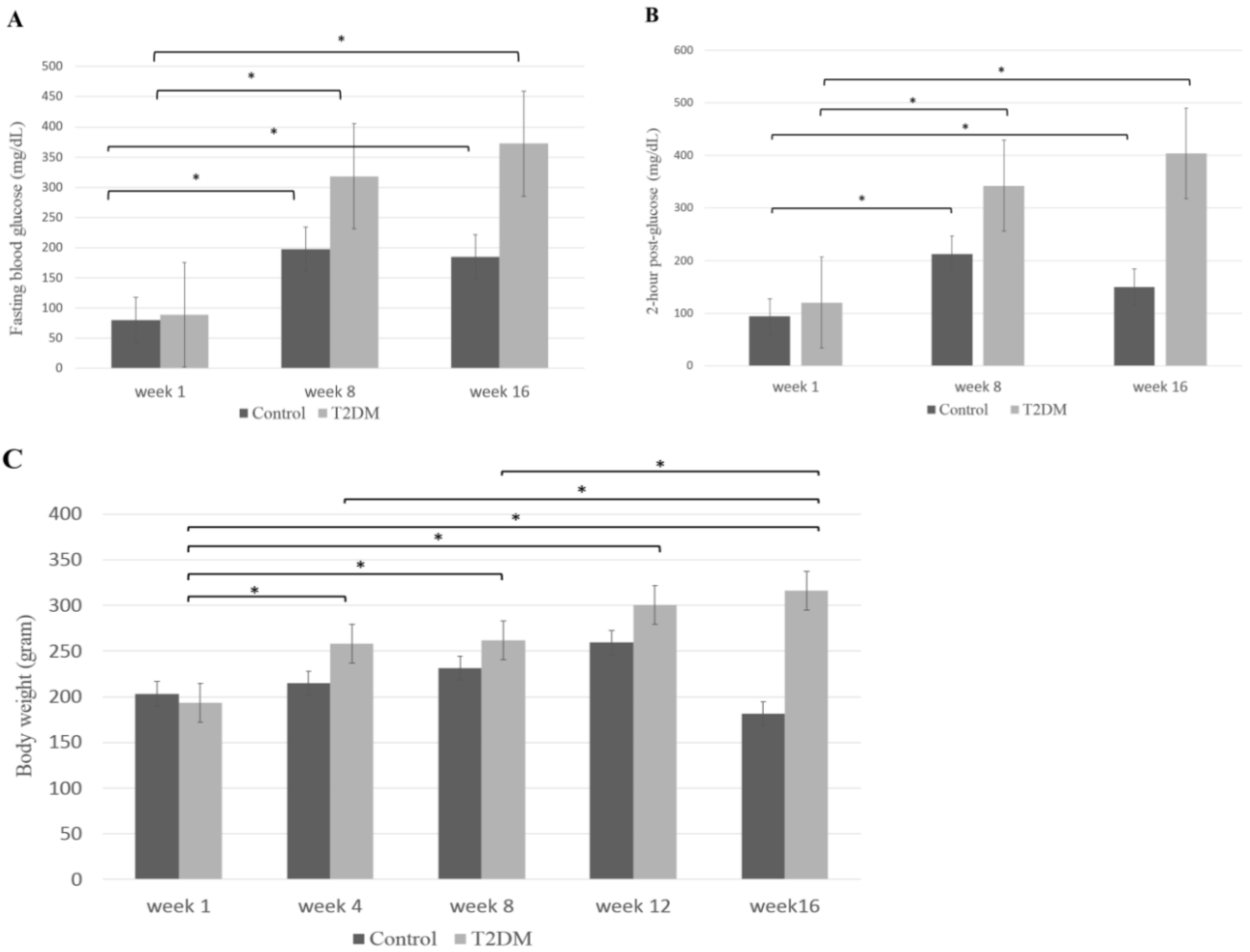

Figure 1. Metabolic validation of type 2 diabetes mellitus in rats after 16 weeks. **A**: Fasting blood glucose levels, **B**: Plasma glucose concentrations at 2-hour post-glucose load, and **C**: Body weight progression during the experimental period. Data are presented as mean ± SD (control, n = 4; T2DM, n = 8). Fasting blood glucose levels **(A)**, 2-hour post-glucose concentrations **(B)**, and body weight **(C)** were significantly higher in the T2DM group compared with the control groups (*$p < 0.05$).

Histological alterations

Histological analysis revealed distinct morphological changes in the skin of diabetic rats (Figure 2A-2B). The dermal thickness was markedly increased in the T2DM group (1091.0 ± 210.9 µm) compared to the control group (803.8 ± 163.9 µm; $p < 0.05$; Figure 2C), while the epidermal thickness indicated a non-significant trend toward thickening (37.3 ± 19.1 µm versus 19.4 ± 7.4 µm; $p > 0.05$).

Quantification of fibroblasts on H&E-stained sections illustrated no significant difference in counts between the control and T2DM groups (15.1 ± 5.9 versus 15.8 ± 6.1 cells/HPF; $p > 0.05$), indicating preserved fibroblast counts despite diabetic conditions (Figure 3).

Masson's Trichrome staining indicated a significant reduction in dermal collagen density in the T2DM group compared to the control group (63.0 ± 3.9% versus 74.5 ± 2.3%; $p < 0.05$; Figure 4C), indicating pronounced extracellular matrix degradation.

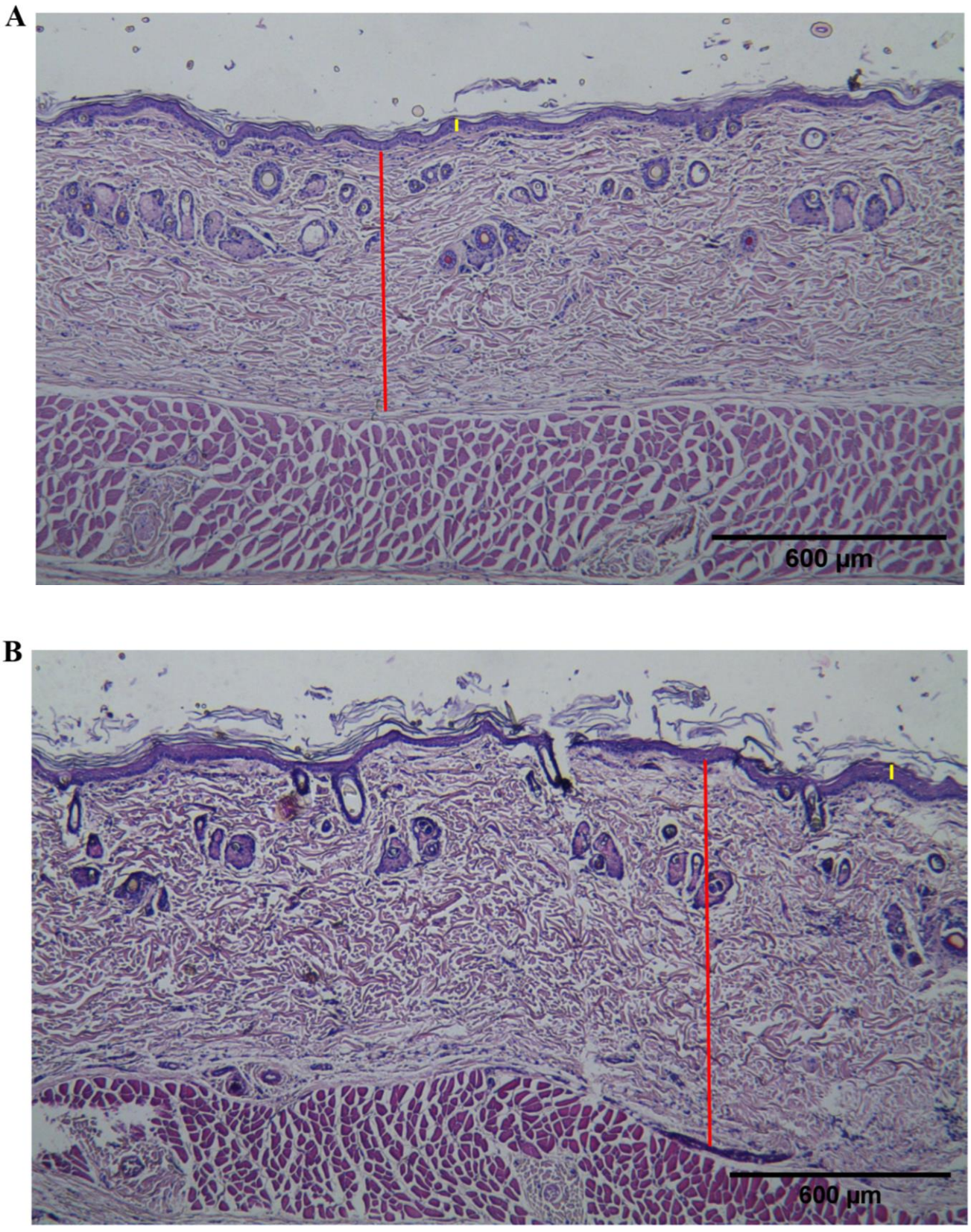

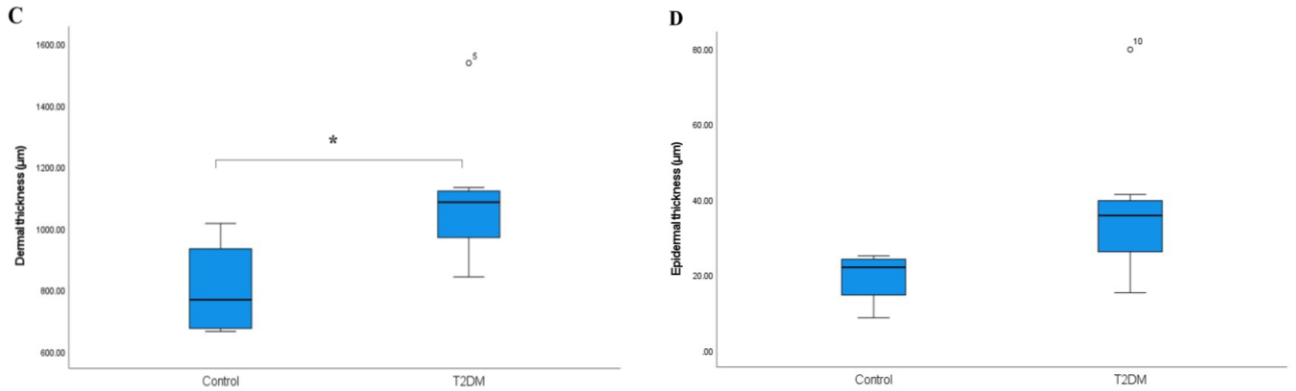

Figure 2. Dermal and epidermal thickness in control and diabetic rats after 16 weeks. **A**: H&E-stained dorsal skin section from the control group, **B**: H&E-stained dorsal skin section from the T2DM group, **C**: Quantitative analysis comparing control and T2DM groups indicated a significant increase in dermal thickness in the skin of diabetic rats (*$p < 0.05$), **D:** Epidermal thickness did not differ significantly between the control and T2DM groups ($p > 0.05$). Images were acquired at 40× magnification, showing dermal thickness (red lines) and epidermal thickness (yellow lines). Data are presented as mean ± SD.

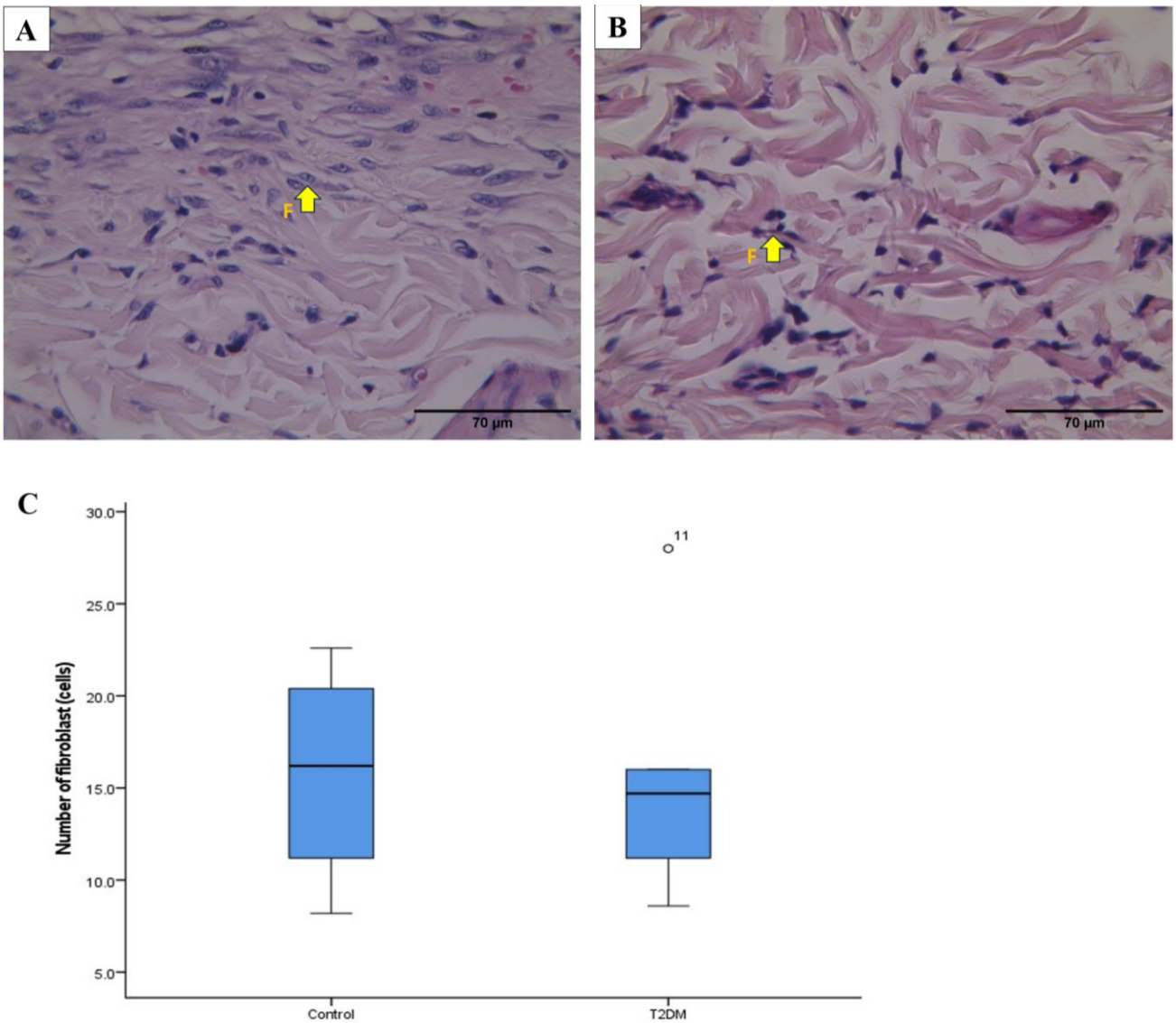

Figure 3. H&E-stained sections showing dermal fibroblasts in control and diabetic rats after 16 weeks. **A**: The control group, **B**: The T2DM group. Fibroblasts (yellow arrows) were identified as the purple spindle-shaped, nucleated cells located between collagen fibers (pink/red). Images were taken at 400x magnification. **C**: Quantitative analysis of dermal fibroblast counts. Fibroblast counts were determined by manually counting fibroblasts in five randomly chosen, non-overlapping high-power fields at 400x magnification per sample. Data are presented as mean ± SD. No significant difference was observed between the control and T2DM groups ($p > 0.05$).

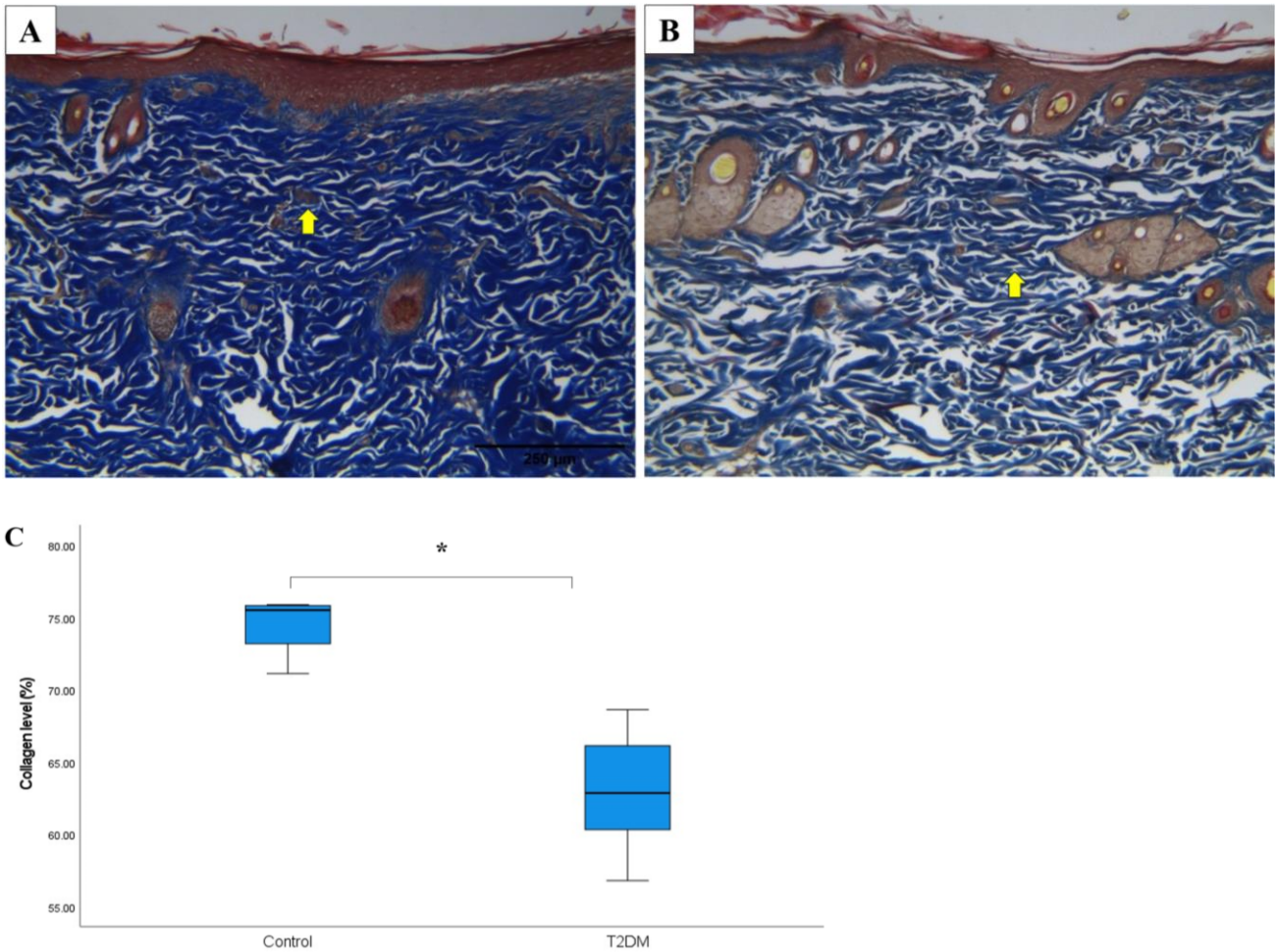

Figure 4. Masson's Trichrome-stained sections of dorsal rat skin after 16 weeks. **A**: Rat skin of the control group showing dense, well-organized dermal collagen fibers. **B**: T2DM (diabetic) rats' skin displaying reduced collagen density and disrupted dermal collagen organization at week 16. Collagen fibers are stained blue (yellow arrows). Images were acquired at 40× magnification. **C**: Quantitative collagen area fraction was analyzed using ImageJ software. Data are presented as mean ± SD. The T2DM group showed significantly lower collagen density compared with the control group (*p < 0.05).

Matrix metalloproteinase-9 levels

Quantitative ELISA analysis demonstrated a significant elevation of MMP-9 protein concentration in the T2DM group compared with the control group (1567.10 ± 935.05 pg/mg protein versus 151.39 ± 68.28 pg/mg protein; $p < 0.05$; Figure 5).

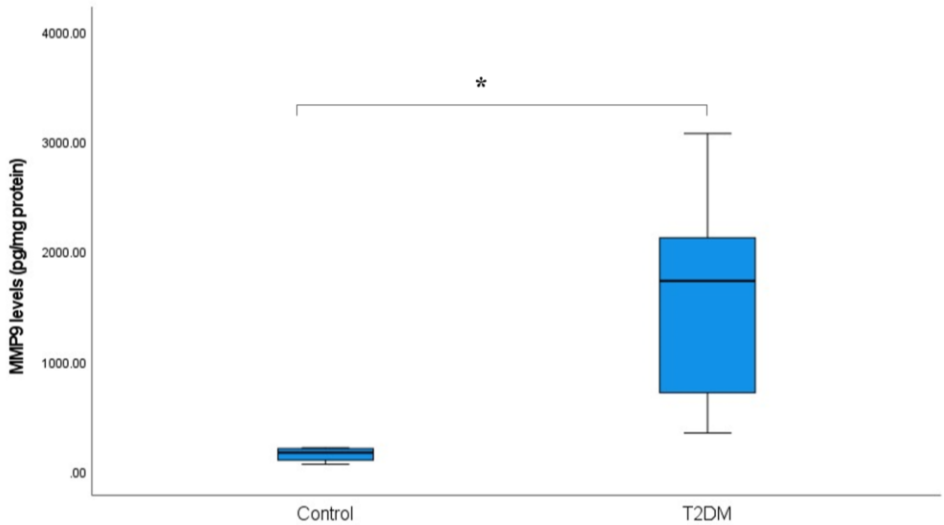

Figure 5. Elevated matrix metalloproteinase-9 concentrations in the skin of diabetic rats after 16 weeks. Data are presented as mean ± SD. The T2DM group showed significantly higher MMP-9 levels compare with the control group (* p < 0.05)

DISCUSSION

The present study demonstrated that T2DM was related to structural and molecular changes in the skin, which align with characteristics often observed in accelerated skin aging in experimental models. The observed sustained hyperglycemia, increased body weight, elevated MMP-9 levels, dermal thickening, and reduced collagen density indicated that chronic metabolic stress was linked to protease-related ECM remodeling, which may lead to premature aging-like skin changes. Sustained hyperglycemia, indicated by elevated FBG and increased 2-hour post-glucose levels, confirmed the development of a T2DM-like metabolic condition phenotype. This chronic metabolic imbalance provides a biologically relevant background for interpreting the progressive skin alterations observed in the present model (Barrière et al., 2018; Brito et al., 2025). Although the control group was maintained on a standard diet, fasting glucose levels were slightly increased but remained within the typical reference ranges observed in non-experimental settings. This may reflect age-related metabolic drift and strain-specific variability commonly observed in Sprague-Dawley rats under laboratory conditions. All groups were housed and handled identically; therefore, intergroup comparisons remain internally valid. Nevertheless, the elevated baseline values were taken into account when interpreting absolute glucose levels.

A key finding of the present study was the change in ECM-related parameters, consistent with improved matrix degradation. The notable decrease in dermal collagen in diabetic rats coincided with a substantial increase in MMP-9, an enzyme that degrades collagen fragments and basement membrane components. Previous studies indicated that MMP-9 levels increased during hyperglycemia, oxidative stress, and inflammatory conditions common in diabetes (Song et al., 2020; Peng et al., 2021).

In diabetic skin, elevated MMP-9 levels were associated with collagen fragmentation, compromised ECM integrity, and deficient tissue repair. Notably, MMP-9 targeted denatured collagen and gelatine rather than native fibrillar collagen, thereby accelerating matrix turnover instead of directly inhibiting collagen synthesis. Therefore, elevated levels of MMP-9 may provide a biologically plausible pathway linking chronic metabolic dysregulation to the structural dermal changes observed in the present study (Quan and Fisher, 2015; Lan et al., 2021).

Histological analysis revealed a notable increase in dermal thickness in diabetic rats, whereas the collagen area fraction was markedly reduced. These findings have been consistently reported in both experimental models and clinical studies of diabetic skin (Verzijl et al., 2000; Poblete Jara et al., 2023). In diabetes, dermal thickening is more a sign of disorganized ECM remodeling rather than an indicator of improved dermal integrity. This difference could be due to the buildup of non-degradable, cross-linked matrix components. The breakdown of collagen by MMPs may occur alongside the deposition of non-collagenous and glycated matrix components, such as AGE-modified collagen, fibronectin, and proteoglycans. The accumulation of these abnormal components can increase tissue volume and stiffness, even in the absence of functional collagen fibers (Gkogkolou and Böhm, 2012; Argyropoulos et al., 2016). Consistent with the present findings, dermal thickening likely resulted from maladaptive matrix remodelling involving both collagen breakdown and the abnormal accumulation of altered EMC components, rather than from collagen accumulation or structural strengthening (Shin et al., 2019). Therefore, the observed decrease in collagen density despite increased dermal thickness can be explained by the accumulation of glycated and disorganized matrix components, which was consistent with the findings of Verzijl et al. (2000) and Zhu et al. (2022).

Although fibroblast counts in the present study did not differ between control and diabetic groups, this finding indicated functional impairment rather than cellular depletion. In diabetic rats, fibroblast counts remained stable, while dermal collagen decreased and MMP-9 levels increased, indicating that ECM changes occurred without a measurable decline in fibroblast numbers. Previous experimental studies have indicated that dermal fibroblasts in diabetic skin are often similar to those in healthy controls; however, dermal fibroblasts in diabetic skin demonstrate morphological and functional abnormalities (Wang et al., 2006; Zhou et al., 2021). Fibroblasts exposed to high-glucose or diabetic environments have been shown to develop a senescence-like phenotype characterized by decreased proliferation, changed morphology, and lower type I collagen production (Nan et al., 2025). Meanwhile, increased expression of MMPs, including MMP-9, has been observed in diabetic fibroblasts (Zhou et al., 2021; Zhu et al., 2022). Therefore, the coexistence of unchanged fibroblast counts with collagen depletion and increased MMP-9 in the present finding indicated a pattern of fibroblast dysfunction rather than fibroblast loss, although direct functional assays were not performed.

In contrast to the noticeable dermal changes, epidermal thickness did not differ between the diabetic and control groups during the present study. The epidermal thickness finding demonstrated that during the 16-week observation period, diabetic rats exhibited minimal measurable epidermal structural changes, with no remarkable difference in thickness. The lack of epidermal thinning findings did not imply the absence of functional or molecular changes; it only meant that these aspects were not evaluated in the present study. The current results indicated that dermal ECM

parameters were more responsive indicators of diabetes-related skin changes than epidermal thickness, without suggesting a clear timeline for skin aging (Argyropoulos et al., 2016; Miura and Yamashita, 2018).

CONCLUSION

The present study characterized a reproducible preclinical rat model in which type 2 diabetes mellitus was associated with alterations in dermal ECM remodeling. Diabetic rats exhibited reduced dermal collagen density, a significant increase in MMP-9 protein levels, and increased dermal thickness compared to the control group, indicating disrupted matrix homeostasis under chronic metabolic stress. The current findings indicated structural and molecular changes in diabetic rat skin and demonstrated an association between diabetic metabolic state and dermal ECM remodelling. Future studies should expand molecular profiling, incorporate enzymatic activity assays, broader protease profiling, extended time-course analyses, and interventional approaches to further clarify mechanisms and explore potential strategies to preserve ECM integrity.

DECLARATIONS

Acknowledgments

The authors gratefully acknowledge the management of the Department of Chemistry at the Faculty of Medicine, Universitas Indonesia, Jakarta, Indonesia, and the Department of Biochemistry and Molecular Biology, Faculty of Medicine, Universitas Indonesia, Jakarta, Indonesia, for access and permission to use the university's facilities.

Authors' contributions

Ruri Eka Maryam Mulyaningsih and Desak Gede Budi Krisnamurti contributed to the conceptualization of the study, developed the protocols and experimental design, and were responsible for editing and reviewing the manuscript. Neng Tine Kartinah and Ani Retno Prijanti carried out the experimental study and prepared the initial draft of the manuscript. Christian Marco Hadi Nugroho performed the statistical analyses. All authors have read and approved the final version of the manuscript.

Availability of data and materials

The authors confirmed that all data supporting the findings of the present study are included within the manuscript.

Ethical considerations

This manuscript was written by the authors based on original scientific results and has not been published elsewhere. An artificial intelligence tool (Grammarly) was used solely for language editing and grammatical refinement. All scientific content, results, data interpretation, and conclusions were developed independently by the authors.

Funding

This study was conducted without any financial support.

Competing interests

The authors declared no conflict of interest.

REFERENCES

American veterinary medical association (AVMA) (2020). AVMA guidelines for the euthanasia of animals: 2020 Edition. Schaumburg, IL, USA. Available at: https://www.avma.org/resources-tools/avma-policies/avma-guidelines-euthanasia-animals

Argyropoulos AJ, Robichaud P, Balimunkwe RM, Fisher GJ, Hammerberg C, Yan Y, and Quan T (2016). Alterations of dermal connective tissue collagen in diabetes: Molecular basis of aged-appearing skin. PLOS ONE, 11(4): e0153806. DOI: https://www.doi.org/10.1371/journal.pone.0153806

Arnal-Forné M, Molina-García T, Ortega M, Marcos-Garcés V, Molina P, Ferrández-Izquierdo A, Sepulveda P, Bodí V, Ríos-Navarro C, and Ruiz-Saurí A (2024). Changes in human skin composition due to intrinsic aging: A histologic and morphometric study. Histochemistry and Cell Biology, 162(4): 259-271. DOI: https://www.doi.org/10.1007/s00418-024-02305-w

Barrière DA, Noll C, Roussy G, Lizotte F, Kessai A, Kirby K, Belleville K, Beaudet N, Longpré JM, Carpentier AC et al. (2018). Combination of high-fat/high-fructose diet and low-dose streptozotocin to model long-term type-2 diabetes complications. Scientific Reports, 8(1): 424. DOI: https://www.doi.org/10.1038/s41598-017-18896-5

Bradford MM (1976). A rapid and sensitive method for the quantitation of microgram quantities of protein utilizing the principle of protein-dye binding. Analytical Biochemistry, 72(1-2): 248-254. DOI: https://www.doi.org/10.1016/0003-2697(76)90527-3

Berlanga-Acosta JA, Guillén-Nieto GE, Rodríguez-Rodríguez N, Mendoza-Mari Y, Bringas-Vega ML, Berlanga-Saez JO, García del Barco Herrera D, Martinez-Jimenez I, Hernandez-Gutierrez S, and Valdés-Sosa PA (2020). Cellular senescence as the pathogenic hub of diabetes-related wound chronicity. Frontiers in Endocrinology, 11: 573032. DOI: https://www.doi.org/10.3389/fendo.2020.573032

Brito AK da S, Mendes AV da S, Timah AB, Santos Oliveira AS da S, Lopes MJ, Suzuki CA, Prianti M das G, Abreu RR de, Lucarini M, Durazzo A et al. (2025). Experimental models of type 2 diabetes mellitus induced by combining hyperlipidemic diet (HFD) and streptozotocin administration in rats: An integrative review. Biomedicines, 13(5): 1158. DOI: https://www.doi.org/10.3390/biomedicines13051158

Brownlee, M. (2001). Biochemistry and molecular cell biology of diabetic complications. Nature, 414(6865): 813-820. DOI: https://www.doi.org/10.1038/414813a

Chen J, Qin S, Liu S, Zhong K, Jing Y, Wu X, Peng F, Li D, and Peng C (2023). Targeting matrix metalloproteases in diabetic wound healing. Frontiers in Immunology, 14: 1089001. DOI: https://www.doi.org/10.3389/fimmu.2023.1089001

Giangreco A, Goldie SJ, Failla V, Saintigny G, and Watt FM (2010). Human skin aging is associated with reduced expression of the stem cell markers β1 integrin and MCSP. Journal of Investigative Dermatology, 130(2): 604-608. DOI: https://www.doi.org/10.1038/jid.2009.297

Gkogkolou P, and Böhm M (2012). Advanced glycation end products. Dermato-Endocrinology, 4(3): 259-270. DOI: https://www.doi.org/10.4161/derm.22028

Kartinah NT, Komara N, Noviati ND, Dewi S, Yolanda S, Radhina A, Heriyanto H, and Sianipar IR (2022). Potential of *Hibiscus sabdariffa* Linn. in managing FGF21 resistance in diet-induced-obesity rats via miR-34a regulation. Veterinary Medicine and Science, 8(1): 309-317. DOI: https://www.doi.org/10.1002/vms3.653

Lan B, Zhang L, Yang L, Wu J, Li N, Pan C, Wang X, Zeng L, Yan L, Yang C et al. (2021). Sustained delivery of MMP-9 siRNA via thermosensitive hydrogel accelerates diabetic wound healing. Journal of Nanobiotechnology, 19(1): 130. DOI: https://www.doi.org/10.1186/s12951-021-00869-6

Liu J, Ren ZH, Qiang H, Wu J, Shen M, Zhang L, and Lyu J (2020). Trends in the incidence of diabetes mellitus: results from the Global Burden of Disease Study 2017 and implications for diabetes mellitus prevention. BMC Public Health, 20(1): 1415. DOI: https://www.doi.org/10.1186/s12889-020-09502-x

Miura K and Yamashita K (2018). Evaluation of aging, diabetes mellitus, and skin wounds by scanning acoustic microscopy with protease digestion. Pathobiology of Aging & Age-Related Diseases, 8: 1516072. DOI: https://www.doi.org/10.1080/20010001.2018.1516072

Moraes VR, Melo MO, and Maia Campos PMBG (2023). Evaluation of morphological and structural skin alterations on diabetic subjects by biophysical and imaging techniques. Life, 13(2): 579. DOI: https://www.doi.org/10.3390/life13020579

Nan L, Guo P, Hui W, Xia F, and Yi C (2025). Recent advances in dermal fibroblast senescence and skin aging: unraveling mechanisms and pioneering therapeutic strategies. Frontiers in Pharmacology, 16:1592596. DOI: https://doi.org/10.3389/fphar.2025.1592596

Nindita Y, Utomo AW, Maharani N, Mahati E, Kristiandi IF, Kesumayadi I, Kurniawati ED, Sobirin MA, and Wijayahadi N **(**2023). Protective effect of Curcuma domestica and Curcuma xanthorrhiza extracts toward kidney, liver, and pancreatic organ dysfunction in streptozotocin-induced diabetes mellitus mice. Natural and Life Sciences Communications, 22(2): e2023029**.** DOI: https://www.doi.org/10.12982/NLSC.2023.029

Ogata Y, Yamada T, Hasegawa S, Sanada A, Iwata Y, Arima M, Nakata S, Sugiura K, and Akamatsu H (2021). SASP-induced macrophage dysfunction may contribute to accelerated senescent fibroblast accumulation in the dermis. Experimental Dermatology, 30(1): 84-91. DOI: https://www.doi.org/10.1111/exd.14205

Pandey S, Chmelir T, and Chottova DM (2023). Animal models in diabetic research—history, presence, and future perspectives. Biomedicines, 11(10): 2852. DOI: https://www.doi.org/10.3390/biomedicines11102852

Peng Z, Nguyen TT, Song W, Anderson B, Wolter WR, Schroeder VA, Hesek D, Lee M, Mobashery S, and Chang M (2021). Selective MMP-9 inhibitor (R)-ND-336 alone or in combination with linezolid accelerates wound healing in infected diabetic mice. ACS Pharmacology and Translational Science, 4(1): 107-117. DOI: https://www.doi.org/10.1021/acsptsci.0c00104

Percie du SN, Hurst V, Ahluwalia A, Alam S, Avey MT, Baker M, Browne WJ, Clark A, Cuthill IC, Dirnagl U et al. (2020). The ARRIVE guidelines 2.0: Updated guidelines for reporting animal research. PLOS Biology, 18(7): e3000410. DOI: https://www.doi.org/10.1371/journal.pbio.3000410

Poblete JC, Nogueira G, Morari J, do Prado TP, de Medeiros BR, Velloso LA, Velander W, and de Araújo EP (2023). An older diabetes-induced mice model for studying skin wound healing. PLOS ONE, 18(2): e0281373. DOI: https://www.doi.org/10.1371/journal.pone.0281373

Powers JC, Asgian JL, Ekici ÖD, and James KE (2002). Irreversible Inhibitors of Serine, Cysteine, and Threonine Proteases. Chemical Reviews, 102(12): 4639-4750. DOI: https://www.doi.org/10.1021/cr010182v

Quan T and Fisher GJ (2015). Role of age-associated alterations of the dermal extracellular matrix microenvironment in human skin aging: A mini-review. Gerontology, 61(5): 427-434. DOI: https://www.doi.org/10.1159/000371708

Sanapalli BKR, Yele V, Singh MK, Thaggikuppe Krishnamurthy P, and Karri VVSR (2021). Preclinical models of diabetic wound healing: A critical review. Biomedicine and Pharmacotherapy, 142: 111946. DOI: https://www.doi.org/10.1016/j.biopha.2021.111946

Schneider CA, Rasband WS, and Eliceiri KW (2012). NIH image to imageJ: 25 years of image analysis. Nature Methods, 9(7): 671-675. DOI: https://www.doi.org/10.1038/nmeth.2089

Shin JW, Kwon SH, Choi JY, Na JI, Huh CH, Choi HR, and Park KC (2019). Molecular mechanisms of dermal aging and antiaging approaches. International Journal of Molecular Sciences, 20(9): 2126. DOI: https://www.doi.org/10.3390/ijms20092126

Song M, Chen L, Zhang L, Li C, Coffie JW, Fang Z, Zhang L, Wang S, Gao X, and Wang H (2020). Cryptotanshinone enhances wound healing in type 2 diabetes with modulatory effects on inflammation, angiogenesis and extracellular matrix remodelling. Pharmaceutical Biology, 58(1): 845-853. DOI: https://www.doi.org/10.1080/13880209.2020.1803369

Van Pelt LF (1977). Ketamine and xylazine for surgical anesthesia in rats. Journal of the American Veterinary Medical Association, 171(9): 842-844. Available at: https://pubmed.ncbi.nlm.nih.gov/924855/

Varani J, Dame MK, Rittie L, Fligiel SEG, Kang S, Fisher GJ, and Voorhees JJ (2006). Decreased Collagen Production in Chronologically Aged Skin. The American Journal of Pathology, 168(6): 1861-1868. DOI: https://www.doi.org/10.2353/ajpath.2006.051302

Verzijl N, DeGroot J, Thorpe SR, Bank RA, Shaw JN, Lyons TJ, Bijlsma JWJ, Lafeber FPJG, Baynes JW, and TeKoppele JM (2000). Effect of Collagen Turnover on the Accumulation of Advanced Glycation End Products. Journal of Biological Chemistry, 275(50): 39027-39031. DOI: https://www.doi.org/10.1074/jbc.M006700200

Wells MY, Voute H, Bellingard V, Fisch C, Boulifard V, George C, Picaut P (2021). Histomorphology and vascular lesions in dorsal rat skin used as injection sites for a subcutaneous toxicity study. Toxicologic Pathology, 38(2): 258-266. DOI: https://www.doi.org/10.1177/0192623309357953

Wlaschek M, Maity P, Makrantonaki E, and Scharffetter-Kochanek K (2021). Connective tissue and fibroblast senescence in skin aging. Journal of Investigative Dermatology, 141(4): 985-992. DOI: https://www.doi.org/10.1016/j.jid.2020.11.010

Zhou P, Yang C, Zhang S, Ke ZX, Chen DX, Li YQ, and Li Q (2021). The imbalance of MMP-2/TIMP-2 and MMP-9/TIMP-1 contributes to collagen deposition disorder in diabetic non-injured skin. Frontiers in Endocrinology, 12:734485. DOI: https://www.doi.org/10.3389/fendo.2021.734485

Zhu P, Chen C, Wu D, Chen G, Tan R, and Ran J (2022). AGEs-induced MMP-9 activation mediated by Notch1 signaling is involved in impaired wound healing in diabetic rats. Diabetes Research and Clinical Practice, 186: 109831. DOI: https://www.doi.org/10.1016/j.diabres.2022.109831